Vol 3 | Issue 1 | Pages 81-94

Advances in Metallurgical and Material Engineering
ISSN: 2689-8705

Research Article

DOI: 10.36959/508/399

Influence of Heat Treatment and Surface Finishing on the Corrosion Behavior of Additive Manufactured Ti-6Al-4V

Mo Li, Dennis Pede, Tobias Poleske and Hadi Mozaffari-Jovein*

Institute for Materials Science and Engineering (IWAT), Furtwangen University Campus Tuttlingen, Germany

Abstract

The present study is to investigate the influence of heat treatment and surface finishing on the corrosion behavior of Ti-6Al-4V alloy produced by selective laser melting (SLM) using potentiodynamic polarization measurements in 0.9 wt.% NaCl at 37 °C. A conventionally fabricated Ti-6Al-4V alloy was used as a comparison. Results show that the surface state plays a critical role in controlling the pitting corrosion resistance, while the impact of the microstructural factors are subsidiary. The order of that is as follows: Polished (SLM/Wrought) > as-built (SLM) > turned (SLM/Wrought) surface. In the case of samples with a comparable surface, the heat treatment-related microstructure such as consisted phase and grain size of α-phase play an important role. Regarding samples post-treated by polishing, the α + β microstructure with higher β fraction and fine grain size of α-phase or the martensitic microstructure show the better pitting corrosion resistance. The elemental analyses using EDS and ICP-MS have revealed that the alloying element Al is preferentially released during the pitting corrosion compared with V.

Keywords

Ti-6Al-4V, Selective laser melting, Corrosion resistance, Surface finishing, Heat treatment

Introduction

Titanium and its alloys, particularly Ti-6Al-4V, produced by conventional technologies are widely used in industries such as in aeronautical and biomedical application due to low density, high specific strength, excellent corrosion resistance and high biocompatibility [1-6]. In recent years, selective laser melting (SLM), as one of the developed innovative additive Manufacturing (AM) technologies, has attracted increasing attention in the industrial manufacturing of titanium and its alloys [7-10]. Using this technology, near-net-shaped, individualized products with complex geometries and functionalized structures or surfaces can be manufactured. SLM is a powder bed-based method, where parts are manufactured layer by layer through a high-power laser that selectively melts certain parts of the powder material based on a 3D computer aided-design (CAD) model [9-12]. SLM-produced titanium parts show comparable or even much better mechanical properties as compared to the conventional fabricated ones [13,14]. However, corrosion resistance of the separts is still an open question, particularly for permanent implant applications, since the corrosion cannot be inhibited in the aqueous environment after the long-term performance, which may lead to clinical complications and/or the failure of the implant [4].

Besides the release of alloying elements as well as corrosion products may cause clinical complications, e.g. vanadium is considered to be cytotoxic [2,4]. Thus, it is important to study whether the corrosion properties of SLM-produced parts can be as good as that of parts fabricated by conventional technologies. Moreover, this powder bed-based process creates parts with a completely different microstructure caused by high cooling rate and complex heat history during SLM processing and rough surface due to residual powder particles which were partially sintered or melted onto the surface [15,16]. Their influence on the corrosion behavior and the need for post-treatment like surface finishing or heat treatment is still unclear. Although the influence of heat treatment, as well as surface finishing, on the corrosion behavior of the SLM-produced Ti-6Al-4V parts have been reported by few researchers, the studies and statements are still limited [17-19]. In this context, it is also crucial to further investigate for full understanding which factors can affect the corrosion behavior of additive manufactured parts.

Consequently, the aim of the present work was to investi-

***Corresponding author:** Mo Li, Institute for Materials Science and Engineering (IWAT), Furtwangen University Campus Tuttlingen, Tuttlingen, Germany

Accepted: April 18, 2020

Published online: April 20, 2020

Citation: Li M, Pede D, Poleske T, et al. (2020) Influence of Heat Treatment and Surface Finishing on the Corrosion Behavior of Additive Manufactured Ti-6Al-4V. Adv Metallurg Mater Eng 3(1):81-94

Table 1: Chemical Composition in wt.% of Ti - 6Al - 4V powder.

Component	Ti	Al	V	Fe	C	O	N	H
Indicative Value (wt.%)	Bal.	5.5-6.5	3.5-4.5	0-0.25	0-0.08	0-0.13	0-0.05	0-0.012

Table 2: Surface treatment and Roughness of investigated Samples.

	Conventional		**SLM**			**SLM HT i at 800°C**		**SLM HT ii at 1000°C**	
	Wrought I	**Wrought II**	**SLM I**	**SLM II**	**SLM III**	**SLM HT i.I**	**SLM HT i.II**	**SLM HT ii.I**	**SLM HT ii.II**
Surface Treatment	Polished	Turned	Polished	Turned	As - Built	Polished	Turned	Polished	Turned
Surface Roughness Ra (µm)	0.066	0.549	0.063	0.424	8.854	0.036	1.019	0.052	0.662

gate the influence of the surface finishing and heat treatment on the corrosion behavior of SLM-produced Ti-6Al-4V parts in 0.9 wt.% NaCl solution at 37 °C and to compare with ones produced by the conventional manufacturing.

Materials and Methods

Sample preparation

In this work, both additive and conventionally manufactured parts were investigated and compared. The conventional Ti-6Al-4V alloy was manufactured externally and provided in the form of rods with a diameter of 9.5 mm that were produced according to ASTM F136-12 [20]. Specimens with a height of approx. 12.7 mm were cut from the rods. A part of the samples (Wrought I) was semi-manually ground up to 2500 grit with silicon carbide (SiC) sheet and polished up to 6000 grit with silicon cloth, while the others (Wrought II) were turned. The SLM-produced Ti-6Al-4V samples were directly made in the form of cylindrical rods with a diameter of 9.5 mm and a height of 12.7 mm. The Concept Laser M lab cusing 100R was used for manufacturing parts made from the CL 41 TI ELI Ti-6Al-4V powder (ELI Grade 23) under an argon gas atmosphere. The chemical composition of the powder is presented in (Table 1). The first (SLM I) and second (SLM II) group of SLM-produced Ti-6Al-4V alloys were polished and turned exactly like the conventional samples, respectively. The third group (SLM III) of the samples were as built without any post-treatment. Moreover, some SLM-produced Ti-6Al-4V alloys were heat-treated in the Argon gas atmosphere either at 1000 °C for 1 hour (SLM HTi) or at 800 °C for 2 hours (SLM HTii) and then furnace cooled (FC). At last the lateral surfaces of them were also polished and turned. Finally, the surface roughness of all the above samples was measured five times at different locations using a surface profilometer, which was quantified via arithmetic mean surface deviation (R_a) values as shown in (Table 2). All the samples were cleaned in an ultrasonic bath in ethanol for 15 min, rinsed and dried before conducting the electrochemical tests. Eventually, the frontal and base surfaces were carefully isolated from Electrolyte with an adhesive, while the geometries of the lateral surfaces were measured before the electrochemical tests were carried out.

Electrochemical tests

The electrochemical tests were carried out using a potentiostat in a conventional three-electrode-cell. A 0.9 wt.% NaCl solution was prepared with Ultrapure deionized Water (Resistivity ≥ 18.2 MΩ·cm at 25 °C) for electrochemical tests. A graphite rod and a Silver Chloride electrode (Ag/AgCl/3M KCl) were selected as a counter and a reference electrode, respectively. Before electrochemical measurements, the electrolyte was bubbled with nitrogen gas at 37 ± 1 °C for 30 min. According to DIN ISO 10993-15 [21], the samples as the working electrode were put in 0.9% NaCl for two hours to attain the stable state for measuring the open circuit potential (OCP) of the samples. The potentiodynamic polarization measurement was carried out at a sweeping range from -0.5 V to 3 or 6 V versus OCP voltage at a constant sweep rate of 1 mV/s. According to DIN ISO 10993-15, the end potential of 3 V for the study of biomaterials is enough [22]. However, the end potential was set up to 6 V to study the specific differences and the corrosion behavior under the pitting corrosion between the different Ti-6Al-4V samples with polished surfaces as under this condition pitting corrosion potentials can be reached much higher than 3 V. The temperature was set at 37 ± 1 °C with a thermostat bath during the whole test. It is noted that all reported potentials are referred to Standard Hydrogen Electrode (SHE). After the electrochemical tests, the electrolytes were stored in plastic bottles (PP or HDPE) until Inductively Coupled Plasma - Mass Spectrometry (ICP-MS) analysis.

Phase analysis and surface morphology

Phase analyses of all investigated samples were performed by Bruker D8 Discover X-ray diffraction (XRD) using a Cu Kα radiation with a scanning rate of 0.04 °/s in the scanning range of 2θ from 30° to 80°. The microstructures as well as surface morphologies after the electrochemical tests were examined by the digital optic microscopy (OM) and scanning electron microscopy (SEM, Zeiss EVO MA 15) using backscattered electrons (BSE). Chemical analysis of either corroded or not corroded area corresponding with the chemical maps was carried out by Energy-dispersive X-ray spectroscopy (EDS) using a Bruker SDD-EDS detector.

Release of Al and V ions in the solution

The Instrument of Thermo Scientifc™ iCAP™ RQ ICP-MS with SC-4DX Autosampler was used in this work for analysis the concentration of released ions in the electrolyte during an electrochemical test. The analysis of ICP MS was performed in a kinetic energy discrimination (KED) mode with helium as

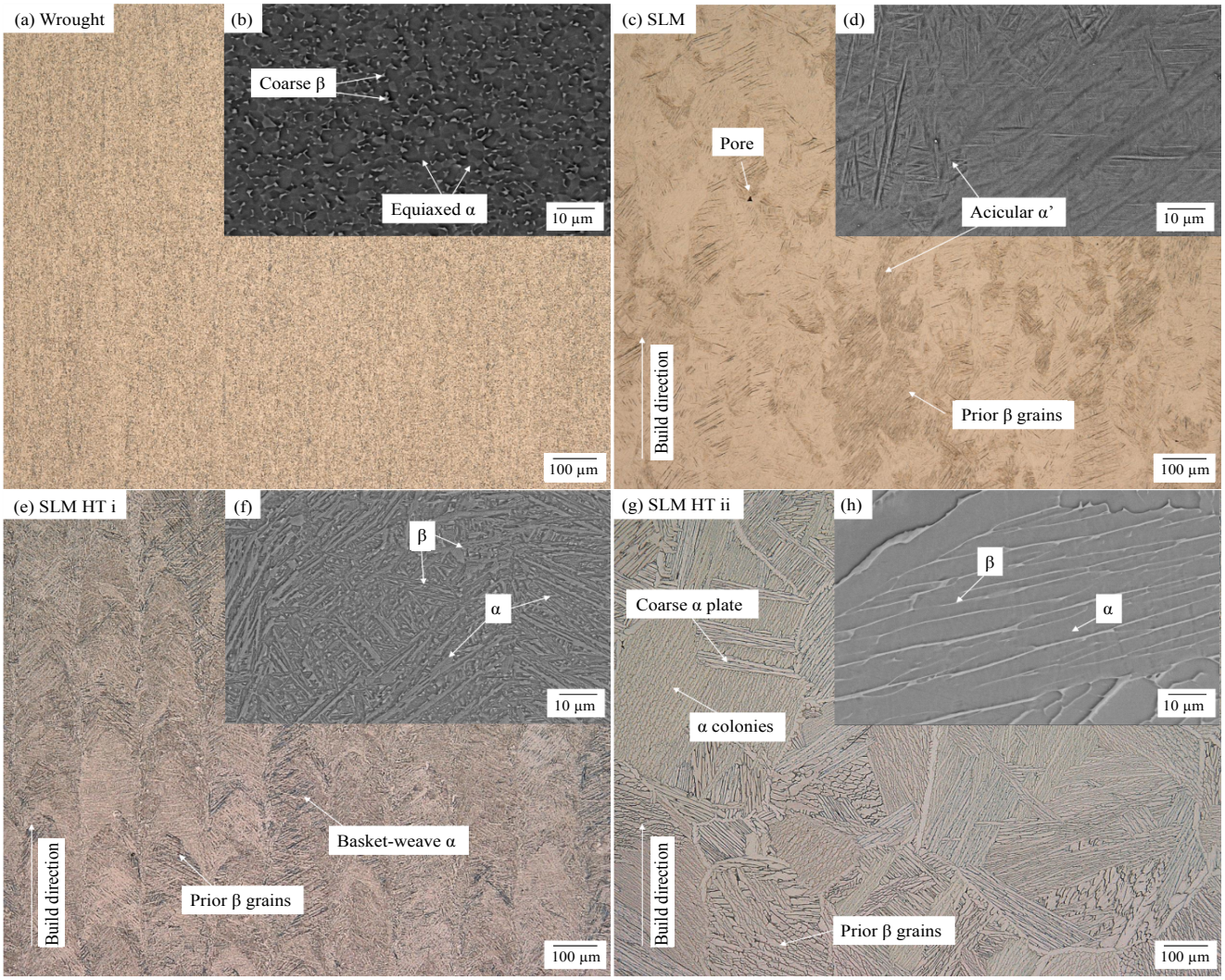

Figure 1: OM (a, c, e, and g) and BSE (b, d, f, and h) micrographs of conventional (a, b), SLM-produced (c, d) and heat-treated at 800 °C (e, f) and at 1200 °C (g, h) samples.

a collision gas. The calibration solutions were prepared with 10 µg/mL certified Al and V single-element standard solutions (Inorganic Ventures). The Ge single-element standard (Inorganic Ventures) were selected as intern standard. High purity nitric acid 67-69% with trace metallic analysis reagent grade and ultrapure deionized Water obtained from the Simplicity UV system (Millipore), were used to prepare dilutions of the samples, standards, and blanks (2% nitric acid). After the electrochemical tests, the obtained solutions were diluted three times with 2% nitric acid. All the plastic solution containers (PP) were rinsed with 2% nitric acid at least twice and dried prior to use.

Results and Discussion

Phase analysis

The α + β microstructure of conventionally fabricated sample Wrought I consists of equiaxed α grains with the size range of 1 to 5 µm and remained β-phase surrounding the α-phase (s. Figure 1a and Figure 1b). A software-aided phase analysis shows a relatively high-volume faction of β-phase with 16.85%. In the case of SLM-produced samples, the prior β-phase has obviously grown over multiple deposited layers along the build direction, while inside the prior β grains a large amount of acicular martensitic α´-phase with the length of several to several tens even to hundreds micrometer was formed due to the high cooling rate of at least 10^3 K/s during the SLM process (s. Figure 1c and Figure 1d). Even under a high magnification (s. Figure 1d), the β-phase could not be seen, which indicates that the residual β-phase particles may be in the nano scale or even does not exist [19]. It was further observed that the martensitic α´-phase was transformed into the basket-weave α + β-phase inside the prior β grains after the heat treatment at 800 °C for 2h with the furnace cooling as shown in (Figure 1e and Figure 1f) [7,18,19]. The length of α grains has a range of 3 to 120 µm. A typical α + β microstructure consisting of coarse prior β gains in the order of 120 to 650 µm in diameter and α plate colonies was obtained after heat treatment at 1200 °C with a low cooling rate (Figure 1g and Figure 1h). Primary α-phase as plates grows along the prior β-phase at the grain boundary region, while α plate colonies with the size range from 100 to 500 µm formed within prior β gains during slow cooling below the β-transus temperature. The volume fraction of β-phase with the value

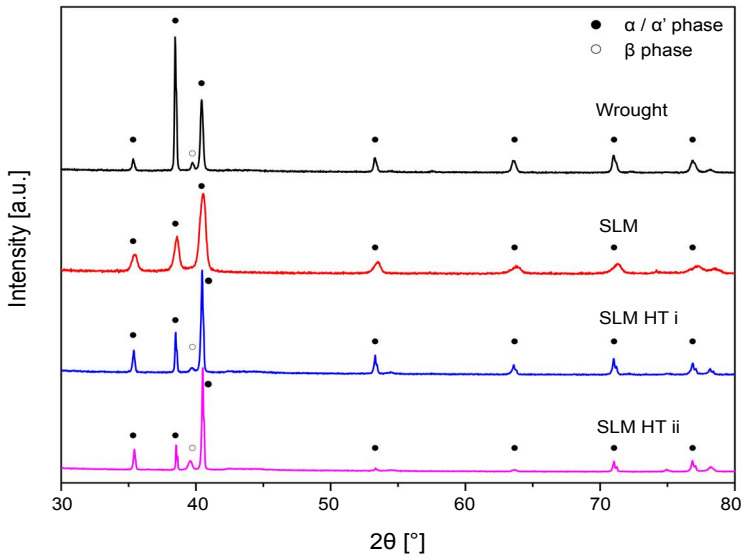

Figure 2: XRD patterns of conventionally produced, SLM-produced and heat-treated SLM-produced samples.

Table 3: Lattice parameters and phase fraction of investigated samples by the Rietveld refinement.

	Lattice parameter α/α´ - phase (nm)		Phase fraction α/α´ - phase (wt.%)	Lattice parameter β - phase (nm)	Phase fraction β - phase (wt.%)
	a	c		a	
Wrought	0.29281	0.46738	82.089	0.32031	17.911
SLM	0.29177	0.46477	/	/	/
SLM HT i	0.29236	0.46677	96.887	0.32040	3.113
SLM HT ii	0.29212	0.46642	84.048	0.32161	15.952

of 15.18% is slightly lower than that of the conventionally produced alloys.

Figure 2 exhibits X-ray diffraction patterns of the conventional, SLM-produced and at 800 °C as well as at 1200 °C heat-treated SLM-produced Ti-6Al-4V samples. According to the XRD analysis the SLM-produced sample consists of either hexagonal close-packed (hcp) α- or α´-phase, the exact determination is not possible solely by XRD as both phases consist of the hcp crystal structure. Only in combination with the metallographic analysis, the phase can be determined as the α´-phase. The pronounced α´-phase peak broadening is likely caused by the raised lath thickness and decreased microstrain, which is related to the formation of α´ martensite [19,23]. Without an obvious β characteristic peak in SLM-produced sample, it suggests that the phase transformation from α´ to β-phase was not detectable by XRD, as shown in microscopy. The lattice parameters of a and c and the α/β-phase fraction of the investigated samples from the results of Rietveld refinement through the software TOPAS (Bruker) are listed in (Table 3). α/α´-phase displays here lower lattice parameters of a and c compared to α-phase in pure titanium with a = 0.29506 nm and c = 0.46835 nm caused by the replacement of titanium atoms by aluminum and vanadium atoms with a smaller atom radius [24].

Electrochemical properties

Figure 3 shows the potentiodynamic polarization curves of conventional, SLM-produced and heat-treated Ti-6Al-4V samples post-treated by polishing after 2h of immersion in a 0.9% NaCl solution at 37 °C. It is characteristic of all polished samples that they a typical stable passivation region due to the formation of a protective TiO_2 passive film within a range of 0.28-1.89 V, the exact values differ slightly among the different samples. Moreover, in this passivation area, the current densities of all polished samples are constant with the increased potential. The similar passivation current densities of 3.5 - 4.5×10^{-6} A·cm^{-2} for SLM-produced samples and of 3.5 - 4.5×10^{-6} A·cm^{-2} for the conventionally manufactured sample (Wrought 1) implies that the dissolution rate of the formed oxide filmat the potential up to 1.89 V independent of the manufactured method can be comparable (Supplementary Table 1).

As the potential increases, the peaks occur near at a potential of 2 V, which may be attributed to a compositional change of the passivation film [25,26]. After the second peak until the potential up to 3.0 V the current density remains constant from 4.67 × 10^{-6} A·cm^{-2} (Wrought I) to 5.02 × 10^{-6} A·cm^{-2} (SLM ii.I), which is related to the second passivation area. When the potential increases over 3.0 V, the current density raises slowly until stable pits form. The

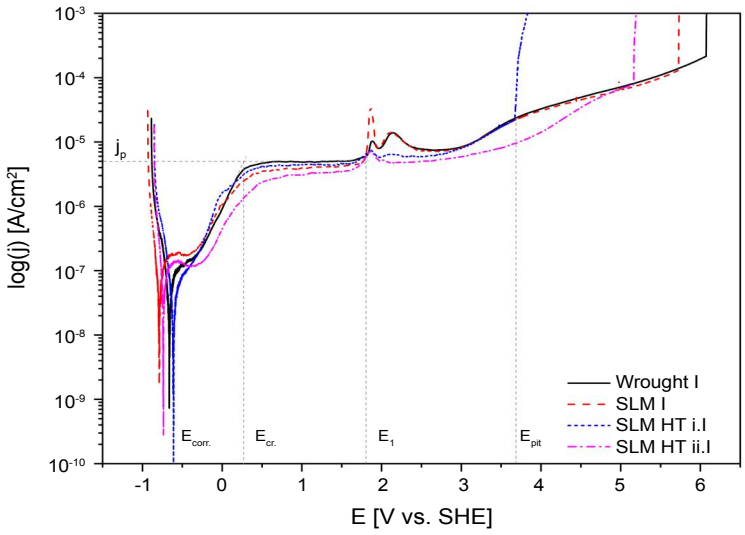

Figure 3: Potentiodynamic polarization curves (to 6V) for the conventionally produced, SLM-produced and heat-treated SLM-produced samples with polished Surfaces.

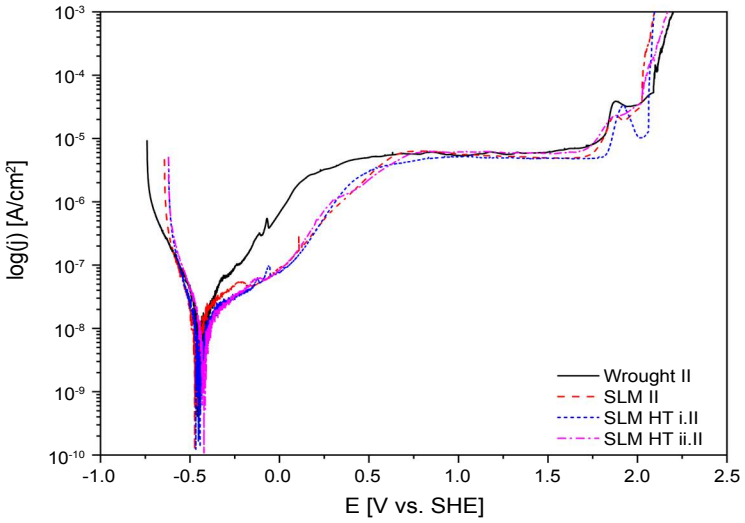

Figure 4: Potentiodynamic polarization curves for the conventionally produced, SLM-produced and heat-treated SLM-produced samples with turned Surfaces.

clear difference between the pitting potentials indicates that the type of constituent phase could play an important role in the resistance to pitting corrosion of the investigated samples. In the case of the samples consisting α + β phase, wrought I clearly displays the most positive pitting corrosion potential with the value of 6.49 V, while SLM HT i. I illustrates the most negative pitting corrosion potential of 3.67 V. This can be related to the higher content of β-phase in wrought I and the greatly smaller in SLM HT i. I, respectively, as shown in the phase analysis, since a more stable oxide film on the β-phase hinders the dissolution and benefits the corrosion resistance due to the higher content of V in comparison to the α-phase [18,27,28]. However, SLM HT ii.I with a similar β-phase content demonstrates a worse resistance to pitting corrosion than Wrought I, which is probably due to the finer grain size of the sample Wrought I [29,30]. On the other hand, SLM I consisting α´-phase shows the second-highest positive pitting corrosion potential of 5.73 V. This may be attributable to the α´ martensite. Owing to the rapid cooling during the SLM-process almost no elemental diffusion could occur. Therefore, a more homogenous elemental distribution can be found in the α´ martensite, resulting in the formation of a more compact and homogeneous oxide on the α´-phase [27,28].

The electrochemical polarization curves of the turned samples are shown in (Figure 4). The critical potential of Wrought II is clearly more negative in comparison to the other turned SLM-produced samples (Supplementary Table 2). The passive current density remains relatively constant with the valve of approx. 5.5×10^{-6} A·cm^{-2} in the first passivation area, which is followed by the current density increasing caused by the oxygen evolution and the phase change in the TiO_2 passive film [25]. Before the formation

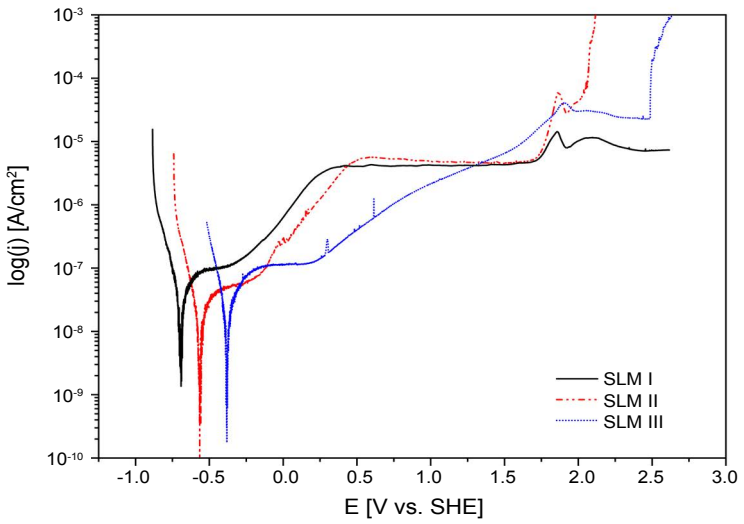

Figure 5: Potentiodynamic polarization curves (to 3 V) for SLM-produced samples with polished (SLM I), turned (SLM II) and as-built (SLM III) Surfaces.

of the second passivation region, stable pits form and pitting corrosion occurs at 2.03-2.09 V (s. Figure 4). This is the case for all samples with a turned surface, even when the pitting corrosion potentials slightly differ among the samples. The quite similar pitting corrosion potential suggest that the influence of the constituent phase and the microstructure for turned samples is negligible.

In the case of as-built SLM sample without surface treatment (SLM III) as seen in Figure 5, it points out a totally different behavior in the passivation area, namely, in the potential range of 0.2 to 1.8 V it does not show a stable passive region like the other samples. The reason is probably the porous-like outer layer, resulting in a more active surface and eventually a higher current density. In the (micro-) pores on the layer, a large number of corrosion products can be easily formed and lead to an autocatalytic corrosion cell, which is further followed by serious localized metastable pitting [31]. The occurrence of meta stable pitting within the micropore could lead to a slight increase of the anodic current density, at the same time followed by a repassivation of meta stable pitting by the pore wall [31,32]. Another reason for the slow increase in current density in this part could be crevice corrosion resulting from the irregular porous SLM-produced surface [32-34]. As the potential increases over the 1.9 V, a plateau with a current density of 23.41 × 10^{-6} A·cm^{-2} is observed, which is much higher than that of all polished samples. This result implies that the corrosion resistance can be improved by the polishing process.

By contrast of the SLM-produced samples with the three different surface conditions, the surface state may play a significant role in the macroscale for the electrochemical corrosion behavior. The corrosion potential of the SLM-produced sample with the as-built surface is more positive than that of the polished and turned surfaces. This suggests that the original as-built surface should be more thermodynamic stable. Meanwhile, the polished sample shows no pitting corrosion up to a potential of 3.5 V, whereas the as-built and turned surfaces clearly show pitting corrosion. Namely, the polishing process can hinder the breakdown of the oxide film due to the enhanced homogeneity and density. On the other hand, the pitting corrosion resistance of 2.49 V for SLM III with the as-built surface is much better than that of the turned sample of 2.03 V, even though the surface roughness of SLM-produced samples is much higher. Thus, the increasing order of pitting corrosion resistance of surface states on SLM-fabricated samples is in the following sequence: Polished > as-built > turned.

Surface morphology after corrosion test

The micrographs of the investigated polished samples after potentiodynamic polarization tests until 6 V in 0.9 wt.% NaCl electrolyte solution at 37 °C are shown in (Figure 6). The optic micrographs (Figure 6a, Figure 6c, Figure 6e and Figure 6g) clearly show that some areas of the parts were severely corroded at the high potential.

As the magnified BSE images of the corroded area of the invested samples in (Figure 6b, Figure 6d, Figure 6f and Figure 6h) showed, locally cracking subsequently to dissolution processes of the oxide film is responsible for the breakdown of SLM I with its martensite α´-phase microstructure [18]. Concerning the other samples, the breakdown occurs preferentially either interior in the grains for Wroght I and SLM HT i.I orin the grain boundary region for SLM HT ii.I, which indicates a more compact and homogeneous oxide film formed on the martensitic structure that has relatively a high interfacial adherence [18], resulting in an improvement of the pitting corrosion resistance. Furthermore, galvanic corrosion at the α/β boundaries either in the prior β grain boundaries or in the α colonies can clearly be observed for the sample SLM ii.I (s. Figure 6g and Figure 6h). Ti-6Al-4V as one of the α + β alloys consists of the alloying elements Al as an α stabilizer and V to stabilize the β-phase [6]. SLM ii.I was heat-treated at 1200 °C and slowly cooled to allow enough time for the partitioning of alloy elements to the respective phases. Therefore, α-phase is enriched in α-stabilizing element (Al), while V segregate

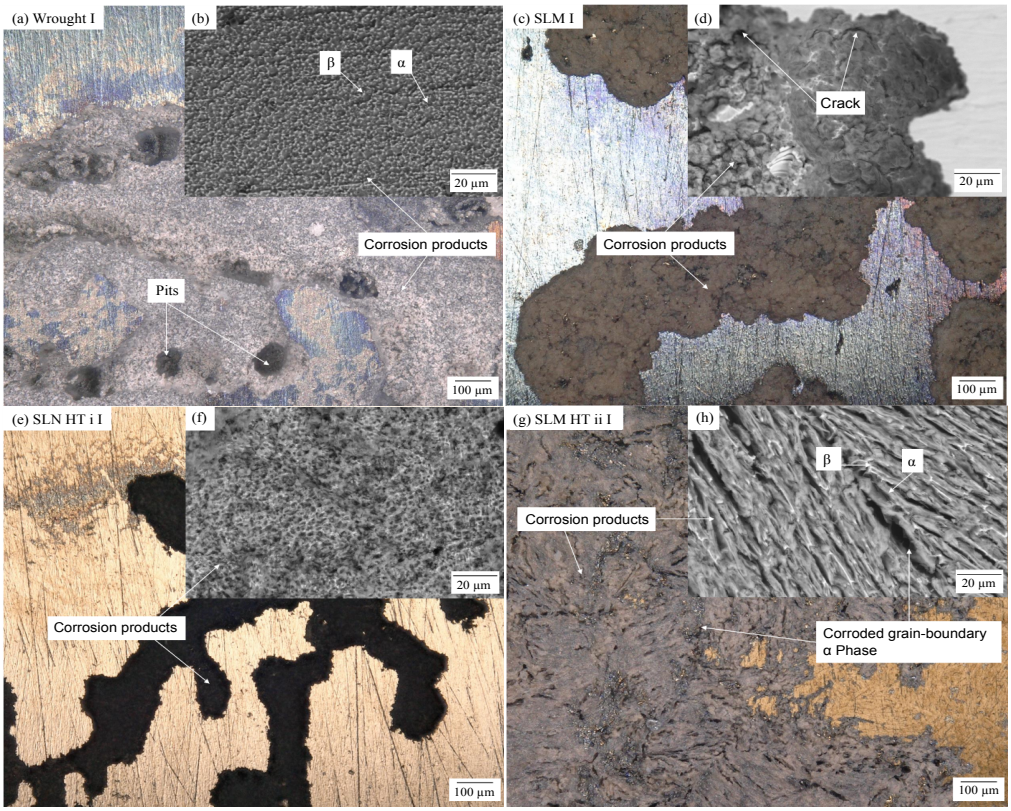

Figure 6: OM (a, c, e, and g) and BSE micrographs (b, d, f, and g) of conventionally produced (a, b), SLM-produced (c, d) and heat-treated at 800 °C (e, f) and 1200 °C (g, h) SLM-produced samples with polished surfaces after electrochemical tests (to 6 V), related to (Figure 3).

into the β-phase. Since the content of alloy elements Al and V in α- and β-phase is different, a galvanic microcell could be created at the α/β boundaries, that can further lead to galvanic corrosion. According to Chen and Tsai, the dissolution rate of β-phase due to the higher V content is slower than that of α-phase [35]. Thus, the β-phase serves as the galvanic cathode. Meanwhile, the edge of α-phase corroded at a faster rate than that at the center. This mechanism and its relevance for additive manufactured parts will be investigated in further studies (Supplementary Table 3).

Consequently, the fraction of β-phase for the samples with the α + β-phase should play an important role in the pitting corrosion. Song, et al. suggested that the β-phase cannot only act as galvanic cathode but also a corrosion barrier depended upon the fraction of β-phase on the exposed area [31]. If the β fraction on the initial exposed surface is small, the β-phase acts mainly as a galvanic cathode and promotes the overall corrosion of α-phase due to selective dissolution and galvanic effect, as shown in Figure 6f SLM HT i.I. During the corrosion, the β-phase fraction on the actual surface can increase and get higher than that at the beginning of corrosion because of the dissolution of α-phase. If the fraction is high enough, the β-phase would serve as an anodic barrier and hinder the corrosion process. In other words, the mainly residual α-phase after the first dissolution would be covered by nets made from continuous β-phase and corrosion products, as shown in BSE micro graphy of Wrought I and SLM HT ii.I in (Figure 6b and Figure 6h), so that the corrosion rate eventually could be greatly reduced.

It has been reported that the grain size distribution effects on the corrosion resistance of titanium alloys. Firstly, an alloy consisting of an α + β microstructure with a finer grain size should have more continuous β phase, if the β-phase fraction is not too low. In this case, the β-phase should serve as an anodic barrier, because the α-phase would be blocked more easily by the continuous β-phase and corrosion products [31]. Moreover, a high density of grain boundary is present in the alloys with fine grain size, that can promote the passivation kinetics and further led to stop the corrosion process because of the rapid formation of a stable passive film [30,36,37]. It is observed that a continuous β-phase net covered on the corrosion area of Wrought I with fine grain size (s. Figure 6a and Figure 6b). Therefore, Wrought I has a more positive pitting corrosion potential due to the refinement grain size compared to SML ii.I with the similar β fraction but a coarser grain size resulted by the low solidification rate.

A comparison within different surface morphologies before and after electrochemical test in the range of -0.5 V to 3 V versus OCP of SLM-produced samples is given in (Figure 7). The absence of a corroded region for the polished sample (see in Figure 7a and Figure 7b) displays that the substrate materials are sufficiently protected by TiO_2 passive film below the potential of 3 V vs. OPC. The turned sample in (Figure 7c and Figure 7d) shows a clearly orientated corrosion profile along the ground tracks, which are resulting from the mechanical turning. One explanation for this is that residual micro-stress is normally stored in the surface layer and near to the surface layer during turning. It has been reported that

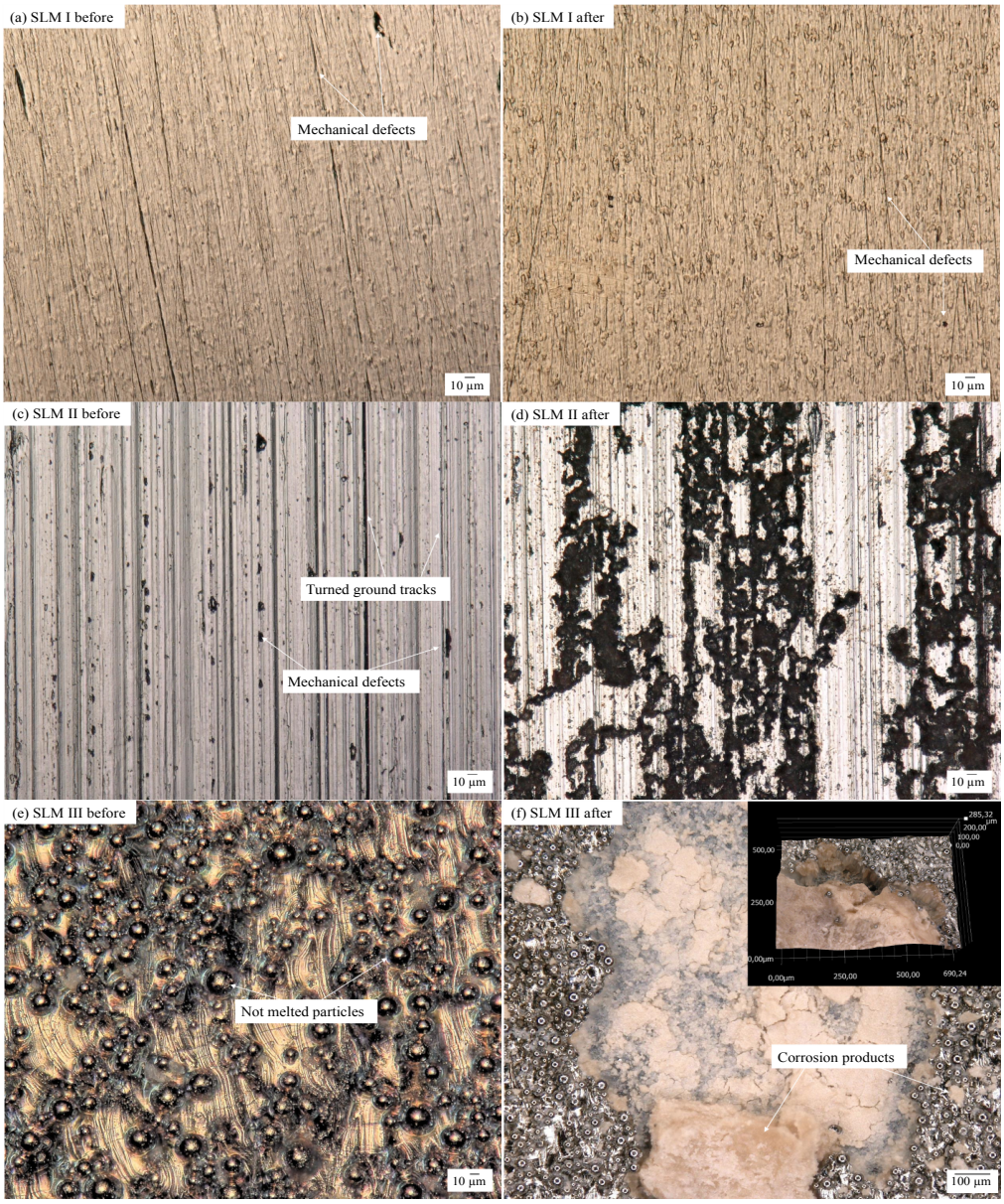

Figure 7: OM micrographs of SLM-produced samples with polished (a,b), turned (c,d) and as-built (e,f) surface states before and after electrochemical tests (to 3 V), related to (Figure 5).

the surface residual stress generated is strongly depending on the machining parameters and the tool geometry [38]. The surface roughness closely regarding the machining process can to some extent reflect the level of the stored residual micro-stress in the surface [38-40]. Especially for the turning process a higher surface roughness usually indicates more surface residual micro-stress, which latter could increase the corrosion rate of the sample [41]. Furthermore, Jang, et al. investigated that machined surfaces have the largest surface residual stress in the hoop direction of cylinders [38]. For this reason, the corrosion pattern was orientated depicted mainly along the hoop.

While the SLM-produced sample prior to the corrosion test has a typical surface morphology with spherical particles that were not or only partially melted and adhered to the substrate during the manufacturing process, the surface after corrosion is characterized by deep pits with irregular shapes and increased corrosion products (in Figure 7e and Figure 7f). The large amount of surface defects for the SLM-produced sample, such as the cavities between the particles and substrate or inclusions with a inhomogeneous distribution of the alloying elements [42], can lead to the stagnation and accumulation of the electrolyte with an increased potential as well as to an autocatalytic corrosion attack, further resulting in the stable corrosion pits [43,44]. Details of the pit geometry at the edge are shown in the inset of Figure 7f. It can be seen that the substrate material is more intensively dissolved during corrosion, whereas the development of pits is clearly hindered by spherical particles at the edge area. This may be caused by a more protecting of oxide film on particles surface and the presence of an inhomogeneous distribution of the alloying elements in the substrate material.

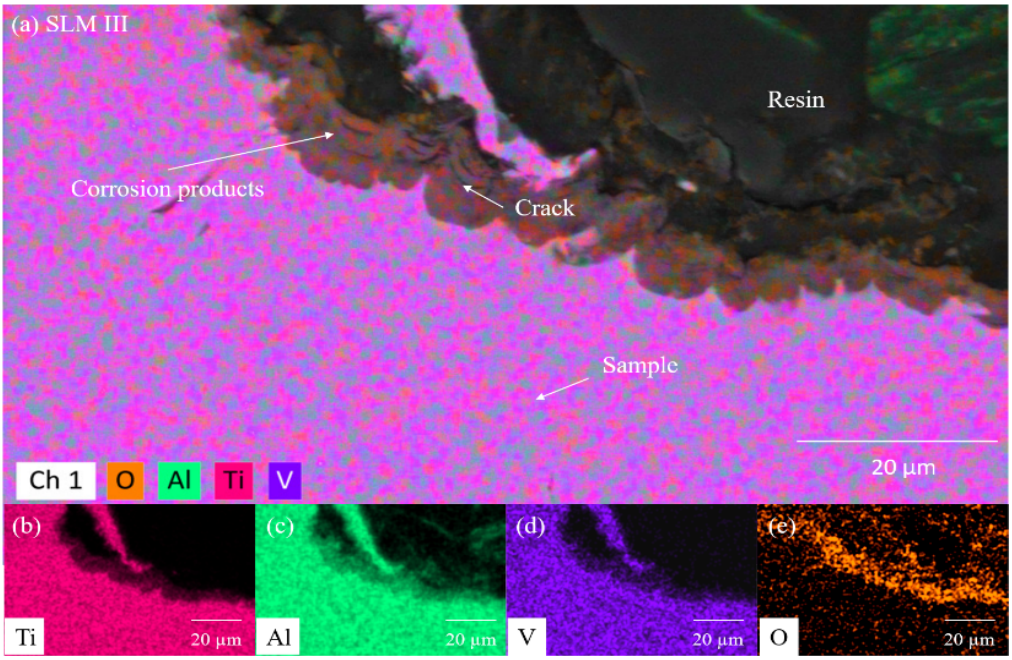

Figure 8: BSE micrograph on the corroded area of the SLM-produced sample with an as-built surface (SLM III) corroded in 0.9% NaCl at 37 °C, cross-section (a) With EDS analysis and corresponding EDS mappings of Ti (b), Al (c), V (d) and O (e) elements.

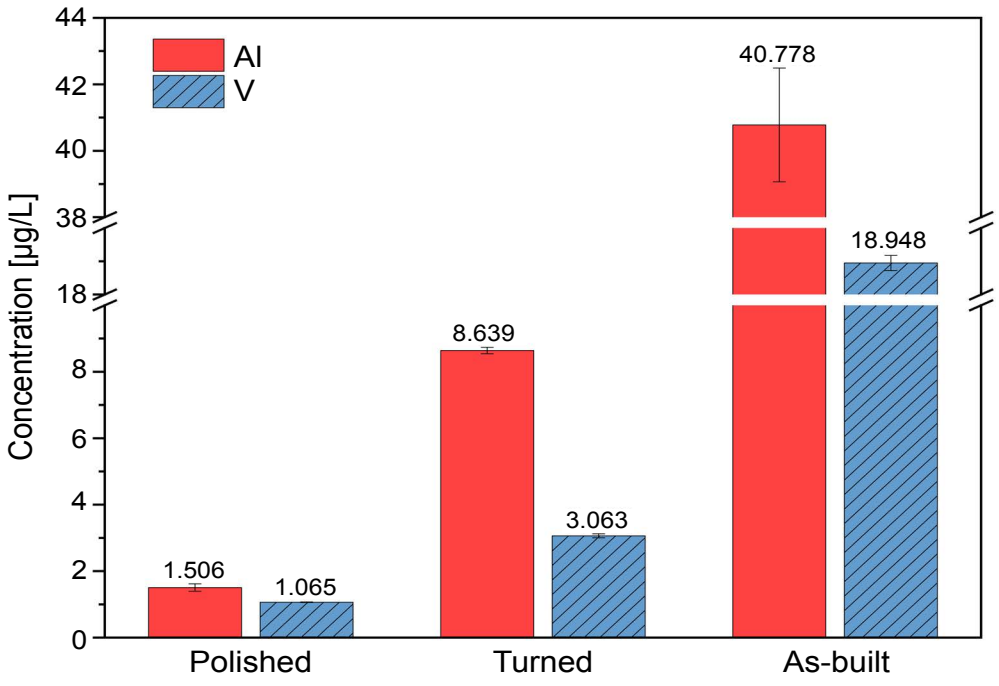

Figure 9: Concentrations of Al and V measured in the electrolyte after electrochemical tests (to 3 V) of the SLM-produced samples with various surfaces, related to (Figure 5).

Release of Al and V ions during the electrochemical tests

The elemental analyses of Al and V measured inside the corroded area on the surface of SLM-produced Ti-6Al-4V samples (s. Figure 8 and Supplementary Table 4) and especially in the electrolytes after performing the electrochemical tests (s. Figure 9) enabled to obtain the information about the potential abilities of alloying elements to release during the potentiodynamic polarization tests. As the EDS maps (s. Figure 8) showed, the alloying elements distribute is uniformly and no significant differences can be seen in the corrosion products as well as in the substrate material. This may be responsible for the martensitic α´-phase consisting of all alloying ele-

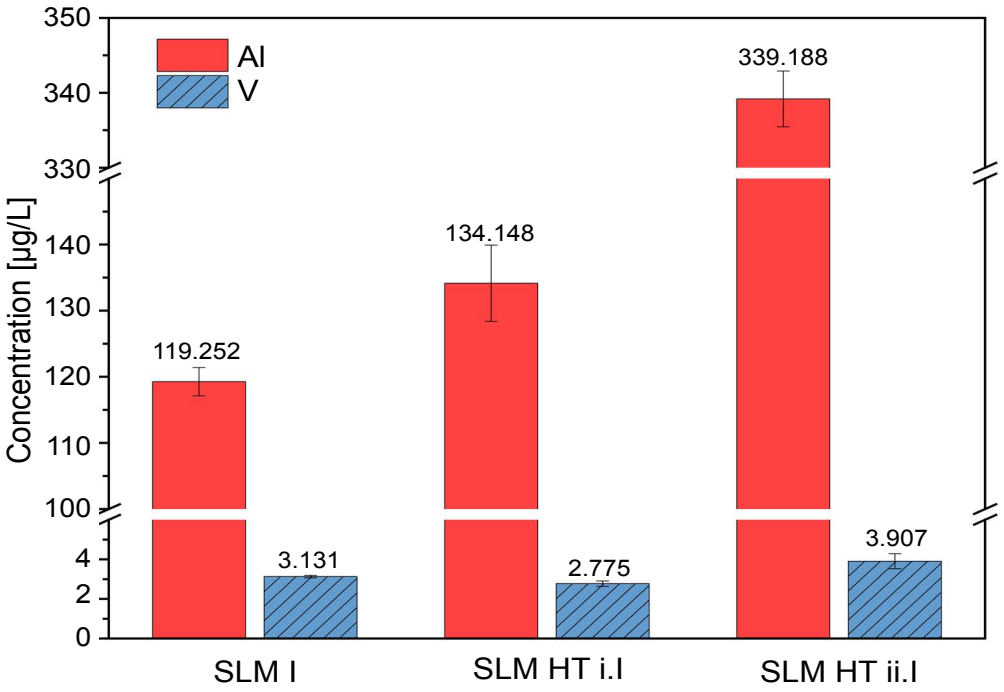

Figure 10: Concentrations of Al and V measured in the electrolyte after electrochemical tests (to 6 V) of the polished SLM-produced samples with and without heat treatments, related to (Figure 3).

ments and can be resulted in a homogenous oxide layer embedded on the surface [45]. This oxide layer can protect the substrate materials against the metal ion Al and V dissolution. However, the ion release is not only caused by the substrate material but can be also generated due to the dissolution of the oxide layer and further induce serious biocompatibility problems such as inflammatory reactions [46,47]. According to the EDS results (s. Supplementary Table 4), more than 66% of the Al content in the SLM III surface (as-built) was dissolved after the polarization tests, while 46% of V was released. Marino, et al. reported similar results, in whose work 30% Al ions of conventionally produced Ti-6Al-4V alloy was released after the corrosion test in a phosphate buffer saline solution at 25 °C, whereas no V was detectable [48]. Moreover, according to Wolner, et al. a complete and dense layer covered by most stable Al_2O_3 cannot be formed at the potential they investigated, since Al has a high solubility resulting in the less dense and irregular thickness of the oxide layer [49]. This can be seen in the Pourbaix diagram of Al for aqueous solutions with the narrow region for stable Al_2O_3 [50]. Meanwhile, the ICP-MS data show that only in case of the breakdown of the passive film the Al/V ratios in the analyzed electrolytes with the value of 2.2 (as-built) and 2.8 (turned) are much higher than that in the chemical composition of the Ti-6Al-4V alloy of 1.5. It is widely accepted that the protective oxide film on the Ti-6Al-4V alloy surface is mainly thermodynamically stable TiO_2 enriched with small amounts of TiO and Ti_2O_3 presented as suboxides in the inner layer [1,46,47,51]. Al and V are present in the oxidation states Al_2O_3, V_2O_3, and V_2O_5, respectively [47,51]. Al_2O_3 was mainly observed at the outer oxide/solution interface [47,52], while the small amount of vanadium oxidizes was always found at the outermost surface [51]. These above elemental analyses suggest that the dissolution of Al_2O_3 in the aqueous solution in the pitting corrosion process was preferential as compared to Vanadium oxidizes, i.e. the Al element should play an important role in the reducing the corrosion resistance of SLM-produced Ti-6Al-4V alloys.

The measurements of metal ion solution for the heat-treated SLM-produced samples with polished and turned surfaces after the potentiodynamic polarization tests till the pitting corrosion are shown in (Figure 10 and Figure 11), respectively. The Al/V ratios in all these electrolytes are more than 1.5 and the concentrations of V ion present at a minor level. This result is consistent with the analysis of the SLM-produced samples with various surfaces. Namely, as compared with V ion, the Al ion is preferentially released during pitting corrosion independent of surface finishing and heat treatment. In the case of the polished samples, (Figure 10) shows the electrolyte of SLM I has the lowest concentration of Al ion. This can be related to the different microstructure of the samples after heat treatment. At first, as mentioned above a homogeneous oxide layer can be formed on the α´-phase of SLM I to protect the metal ion dissolution. Secondly, the galvanic corrosion in the α + β microstructure of the heat-treated samples (SLM i.I and SLM ii.I) can accelerate the corrosion of α-phase. Thus, more Al ion were found in the electrolytes of the heat-treated samples than that of SLM I. That indicates the decreasing order of phase dissolution in the pitting corrosion process of SLM-produced samples without/with heat treatments is as follow: α´< α. Meanwhile, SLM ii.I with the better pitting corrosion resistance shows the relatively higher dissolution ability of Al ion during the pitting corrosion. This can be responsible to the grain size of α-phase in the a + β microstructure. The coarse α-plates with larger grain size in the

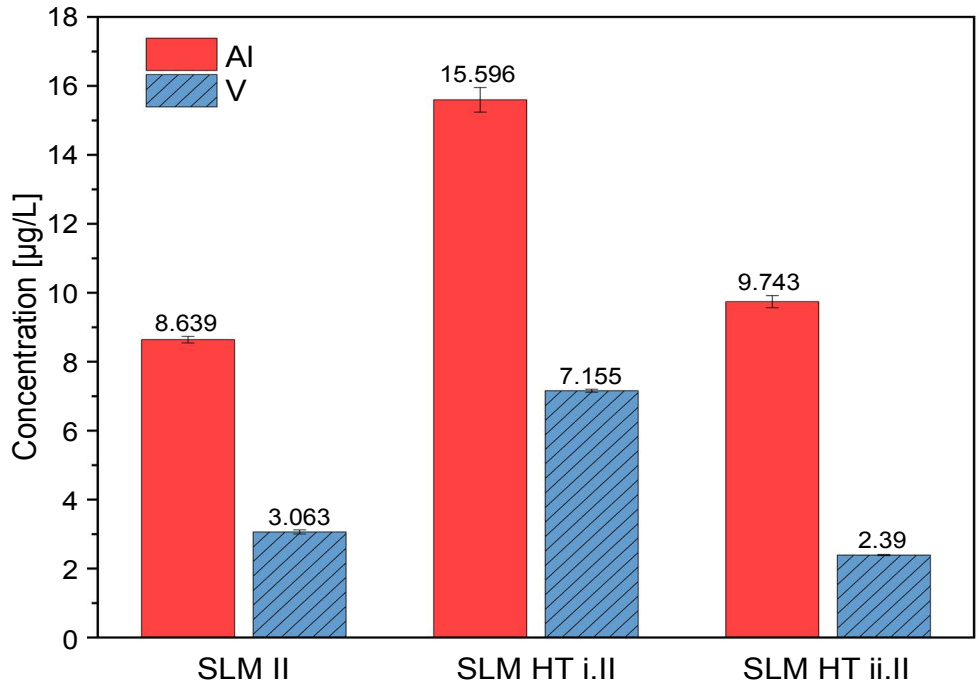

Figure 11: Concentrations of Al and V measured in the electrolyte after electrochemical tests of the turned SLM-produced samples with and without heat treatments, related to (Figure 4).

grain boundaries and inside the prior β grains are observed in SLM ii.I in Figure 1, as compared with SLM i.I. When the pitting corrosion occurs, amounts of Al ion will be released as a large are of α-phase dissolves. The result of the turned SLM-produced samples without/with heat treatment after pitting corrosion show no significant difference in Figure 11. This means, unlike the samples with polished surface the microstructure will not influence on the metal ion Al and V dissolution of the samples with turned surface. The surface state may be as an important factor as well as for the pitting corrosion resistance. The mechanism for this is not clear at the moment and should be further studied.

Conclusions

This study focused on the influence of macro- and microscopic factors namely surface and heat treatmenton the electrochemical behavior of conventionally and SLM-produced Ti-6Al-4V alloys in a 0.9 wt.% NaCl electrolyte solution at 37 °C. The main conclusions can be drawn as follows.

(1) The surface state resulted from the manufacturing process or the surface treatment as a macroscopic factorcan play acritical role in the pitting corrosion behavior of Ti-6Al-4V alloys. The order of pitting corrosion resistance is independent on consisted microstructure for wrought samples as follow: Polished (Wrought I) > turned (Wrought II), in the case of SLM-produced samples that is polished (SLM I) > as-built (SLM III) > turned (SLM II).

(2) The pitting corrosion for samples post-processed by polishing occurs at the high potential (> 3.5 V) and the order of pitting corrosion resistance is Wrought I > SLM I > SLM HT ii.I > SLM HT i.I. In this case, the corrosion behavior can be sensitive to the various micro factors such as contained phases and grain size of α-phase resulted by the produce and heat treatment process. Based on the above analyses, a microstructure consisting of (α + β)-phase with a higher β fraction and finer grain size α-phase or one consisting of more martensite α´-phase can lead to a better pitting corrosion resistance.

(3) Element partitioning is also a main micro factor controlling the corrosion behavior of α + β Ti-6Al-4V alloys, irrespectively of the manufacturing method. Due to the different chemical composition in α and β phases may lead to galvanic corrosion the α/β boundaries, where as the β-phase enriched in V can serve as a galvanic cathode and the α-phase enriched in Al is dissolved preferentially.

(4) According to the results of EDS and ICP MS, the amount of released Al for the SLM-produced samples during the pitting corrosion is much higher compared to V, that indicates a preferential dissolution of Al. Thus, Al should play an important role in declining the corrosion resistance of additive manufactured Ti-6Al-4V.

Acknowledgment

The authors would like to acknowledge the financial support from the Ministry for Education and Research (Bundesministerium für Bildung und Forshung) for this research.

References

1. DM Brunette, P Tengvall, M Textor, et al. (2001) Titanium in Medicine: Material Science, Surface Science, Engineering, Biological Responses and Medical Applications, Springer.

2. E Wintermantel, S W Ha (2009) Medizintechnik Springer Berlin Heidelberg, Heidelberg Berlin.

3. M Niinomi, M Nakai, J Hieda (2012) Development of new metallic alloys for biomedical applications. Acta biomaterialia 8: 3888-3903.
4. C N Elias, J H C Lima, R Valiev, et al. (2008) Biomedical applications of titanium and its alloys. JOM 60: 46-49.
5. M Long, H J Rack (1998) Titanium alloys in total joint replacement-a materials science perspective. Biomaterials 19: 1621-1639.
6. C Leyens, M Peters (2003) Titanium and titanium alloys: Fundamentals and applications. Wiley-VCH Verlag GmbH & Co KGaA.
7. G M Ter Haar, T H Becker (2018) Selective laser melting produced Ti-6Al-4V: Post-Process heat treatments to achieve superior tensile properties. Materials (Basel) 11: 146.
8. Sharon L N Ford (2014) Additive manufacturing technology: potential implications for U.S. manufacturing competitiveness. Journal of International Commerce and Economics.
9. S Liu, C Shin (2019) Additive manufacturing of Ti6Al4V alloy: A review. Materials & Design 164: 107552.
10. B AlMangour (2019) Additive manufacturing of emerging materials. Springer International Publishing, Cham.
11. L A Dobrzanski (2017) Powder metallurgy: Metallurgy - fundamentals and case studies, In Tech Open.
12. B Dutta , F H Froes (2017) The Additive Manufacturing (AM) of titanium alloys. Metal Powder Report, 72: 96-106.
13. H Attar, M Calin, L C Zhang, et al. (2014) Manufacture by selective laser melting and mechanical behavior of commercially pure titanium. Materials Science and Engineering: A 593: 170-177.
14. X P Li, J van Humbeeck, J P Kruth (2017) Selective laser melting of weak-textured commercially pure titanium with high strength and ductility: A study from laser power perspective. Materials & Design 116: 352-358.
15. J Yang, H Yu, J Yin, et al. (2016) Formation and control of martensite in Ti-6Al-4V alloy produced by selective laser melting. Materials & Design 108: 308-318.
16. C Ni, Y Shi, J Liu (2019) Effects of inclination angle on surface roughness and corrosion properties of selective laser melted 316L stainless steel. Materials Research Express 6: 36505.
17. N Dai, L C Zhang, J Zhang, et al. (2016) Corrosion behavior of selective laser melted Ti-6Al-4V alloy in NaCl solution. Corrosion Science 102: 484-489.
18. J Yang, H Yang, H Yu, et al. (2017) Corrosion Behavior of Additive Manufactured Ti-6Al-4V Alloy in NaCl Solution. Metallurgical and Materials Transactions A 48: 3583-3593.
19. Y Xu, Y Lu, K L Sundberg, et al. (2017) Effect of annealing treatments on the microstructure, mechanical properties and corrosion behavior of direct metal laser sintered Ti-6Al-4V. Journal of Materials Engineering and Performance 26: 2572-2582.
20. (2013) ASTM F136-13, Standard Specification for Wrought Titanium-6Aluminum-4Vanadium ELI (Extra Low Interstitial) Alloy for Surgical Implant Applications (UNS R56401). ASTM International, West Conshohocken, PA.
21. Deutsches Institut für Normung e.V., "Biologische Beurteilung von Medizinprodukten - Teil 15: Qualitativer und quantitativer Nachweis von Abbauprodukten aus Metallen und Legierungen," 10.2009, vol. 11.100.20, DIN EN ISO 10993-15.
22. B Burnat, M Walkowiak-Przybyło, T Błaszczyk, et al. (2013) Corrosion behavior of polished and sandblasted titanium alloys in PBS solution. Acta of Bioengineering and Biomechanics 15: 87-94.
23. W Xu, M Brandt, S Sun, et al. (2015) Additive manufacturing of strong and ductile Ti-6Al-4V by selective laser melting via in situ martensite decomposition. Acta Materialia 85: 74-84.
24. L Tretyachenko (2004) Aluminium-Titanium-Vanadium. in Landolt-Börnstein, Numerical Data and Functional Relationships in Science and Technology, Berlin, Heidelberg 11: 26-53, Springer.
25. M Zhu, R Wang, C Chen, et al. (2017) Electrochemical study on the corrosion behavior of Ti 3 SiC 2 in 3.5% NaCl solution. RSC Advances 7: 12534-12540.
26. X Yang, C Du, H Wan, et al. (2018) Influence of sulfides on the passivation behavior of titanium alloy TA2 in simulated seawater environments. Applied Surface Science 458: 198-209.
27. S Y Yu, J R Scully (1997) Corrosion and passivity of Ti-13% Nb-13% Zr in comparison to other biomedical implant alloys. Corrosion Engineering Section 53: 965-976.
28. I Cvijović-Alagić, Z Cvijović, J Bajat, et al. (2014) Composition and processing effects on the electrochemical characteristics of biomedical titanium alloys. Corrosion Science 83: 245-254.
29. L C Zhang, H Attar (2016) Selective laser melting of titanium alloys and titanium matrix composites for biomedical applications: A Review. Advanced Engineering Materials 18: 463-475.
30. S Gollapudi (2012) Grain size distribution effects on the corrosion behaviour of materials. Corrosion Science 62: 90-94.
31. G Song, A Atrens, M Dargusch (1999) Influence of microstructure on the corrosion of diecast AZ91D. Corrosion Science 41: 249-273.
32. B Movahedi (2016) Metallic glasses: Formation and Properties, InTech.
33. R Lage, P Møller, H E Fallesen (2015) The effect of surface treatment and topography on corrosion behavior of EN 1.4404 stainless steel. Materials and Corrosion 66: 1060-1067.
34. G Xie, F Qin, S Zhu, et al. (2014) Corrosion behaviour of porous Ni-free Ti-based bulk metallic glass produced by spark plasma sintering in Hanks' solution. Intermetallics 44: 55-59.
35. J R Chen, W T Tsai (2011) In situ corrosion monitoring of Ti-6Al-4V alloy in H2SO4/HCl mixed solution using electrochemical AFM. Electrochimica Acta 56: 1746-1751.
36. H S Kim, S J Yoo, J W Ahn, et al. (2011) Ultrafine grained titanium sheets with high strength and high corrosion resistance. Materials Science and Engineering: A 528: 8479-8485.
37. D Y Li (2006) Electron work function at grain boundary and the corrosion behavior of nanocrystalline metallic materials. Mater. Res. Soc. Symp. Proc 887.
38. D Y Yang, T R Watkins, K J Kozaczek, et al. (1996) Surface residual stresses in machined austenitic stainless steel. Wear 194: 168-173.
39. E Brinksmeier, J T Cammett, W König, et al. (1982) Residual Stresses-Measurement and Causes in Machining Processes. CIRP Annals 31: 491-510.
40. M Jacobson (2002) Surface integrity of hard-turned M50 steel. Proc Instn Mech Engrs, 216: 47-54.
41. G L Song, Z Xu (2010) The surface, microstructure and corrosion of magnesium alloy AZ31 sheet. Electrochimica Acta 55: 4148-4161.

42. X F Cai, Y P Bao, M Wang, et al. (2015) Investigation of precipitation and growth behavior of Ti inclusions in tire cord steel. Metallurgical Research & Technology 112: 407.

43. J Bhandari, F Khan, R Abbassi, et al. (2015) Modelling of pitting corrosion in marine and offshore steel structures - A technical review. Journal of Loss Prevention in the Process Industries 37: 39-62.

44. A Leon, E Aghion (2017) Effect of surface roughness on corrosion fatigue performance of AlSi10Mg alloy produced by selective laser melting (SLM). Materials Characterization 131: 188-194.

45. M Geetha, U Kamachi Mudali, A K Gogia, et al. (2004) Influence of microstructure and alloying elements on corrosion behavior of Ti-13Nb-13Zr alloy. Corrosion Science 46: 877-892.

46. I Cvijović-Alagić, Z Cvijović, J Bajat, et al. (2016) Electrochemical behaviour of Ti-6Al-4V alloy with different microstructures in a simulated bio-environment. Materials and Corrosion 67: 1075-1087.

47. M Metikoš Huković, A Kwokal, J Piljac (2003) The influence of niobium and vanadium on passivity of titanium-based implants in physiological solution. Biomaterials 24: 3765-3775.

48. C E B Marino, S R Biaggio, R C Rocha Filho, et al. (2006) Voltammetric stability of anodic films on the Ti6Al4V alloy in chloride medium. Electrochimica Acta 51: 6580-6583.

49. C Wolner, G E Nauer, J Trummer, et al. (2006) Possible reasons for the unexpected bad biocompatibility of metal-on-metal hip implants. Materials Science and Engineering 26: 34-40.

50. N TAKENO (2005) Atlas of Eh-pH diagrams: Intercomparison of thermodynamic databases.

51. R N S Sodhi, AWeninger, J E Davies (1991) X-ray photoelectron spectroscopic comparison of sputtered Ti, Ti6Al4V, and passivated bulk metals for use in cell culture techniques. Journal of Vacuum Science & Technology A: Vacuum 9: 1329-1333.

52. C Ciszak, I Popa, J M Brossard, et al. (2016) NaCl induced corrosion of Ti-6Al-4V alloy at high temperature. Corrosion Science 110: 91-104.

Appendix Tables

Supplementary Table 1: The fitting parameters of electrochemical polarization tests of the polished samples.

	$E_{corr.}$ (V vs. SHE)	$E_{cr.}$ (V vs. SHE)	j_p (A/cm²)	E_1 (V vs. SHE)	E_{pit} (V vs. SHE)
Wrought I	-0.674	0.26	3.83×10^{-6}	1.69	6.49
SLM I	-0.791	0.51	4.12×10^{-6}	1.79	5.73
SLM HT i.I	-0.612	0.41	4.48×10^{-6}	1.66	3.67
SLM HT ii.I	-0.739	0.40	3.56×10^{-6}	1.70	5.26

Supplementary Table 2: The fitting parameters of electrochemical polarization tests of the turned samples.

	$E_{corr.}$ (V vs. SHE)	$E_{cr.}$ (V vs. SHE)	j_p (A/cm²)	E_1 (V vs. SHE)	E_{pit} (V vs. SHE)
Wrought II	-0.444	0.30	5.40×10^{-6}	1.80	2.09
SLM II	-0.464	0.68	5.19×10^{-6}	1.87	2.03
SLM HT i.II	-0.447	0.50	5.16×10^{-6}	1.92	2.06
SLM HT ii.II	-0.425	0.72	5.78×10^{-6}	1.72	2.06

Supplementary Table 3: The fitting parameters of electrochemical polarization tests of the SLM-produced sample with an as-built surface.

	$E_{corr.}$ (V vs. SHE)	E_1 (V vs. SHE)	E_{pit} (V vs. SHE)
SLM III	-0.382	1.91	2.49

Supplementary Table 4: Concentrations of Al and V measured on corrosion products and on the not corroded Surface of SLM-produced samples with variours surfaces and heat treatments after electrochemical tests.

Elements	**Ti**	**Al**	**V**		**O**	
Polished	**SLM I**	**Corrosion products**	63.35	1.42	0.91	34.32
(to 6V)		**Sample**	80.65	5.05	1.54	12.76
	SLM HT i.I	**Corrosion products**	49.01	3.38	1.45	46.15
		Sample	85.52	6.64	1.84	6.00
	SLM HT ii.I	**Corrosion products**	59.49	1.07	5.11	34.33
		Sample	80.19	6.53	1.43	11.85
Turned	**SLM I**	**Corrosion products**	58.07	1.53	0.45	39.95
		Sample	88.64	6.78	1.54	3.04
	SLM HT i.I	**Corrosion products**	65.81	2.82	1.61	29.75
		Sample	87.90	6.16	2.56	3.38
	SLM HT ii.I	**Corrosion products**	49.50	3.87	0.49	46.14
		Sample	88.39	5.09	3.81	2.72
As-built	**SLM III**	**Corrosion products**	56.97	2.31	0.91	39.80
		Sample	89.16	6.85	1.69	2.30

DOI: 10.36959/508/399